Norton Equivalent Circuit for Pulsed Photoconductive Antennas-Part I Theoretical Model

Garufo, Alessandro; Carluccio, Giorgio; Llombart Juan, Nuria; Neto, Andrea

DOI
10.1109/TAP.2018.2800524

Publication date
2018

Document Version
Accepted author manuscript

Published in
IEEE Transactions on Antennas and Propagation

Norton Equivalent Circuit for Pulsed Photoconductive Antennas – Part I: Theoretical Model

Alessandro Garufo, *Member, IEEE*, Giorgio Carluccio, Nuria Llombart, *Senior Member, IEEE*, and Andrea Neto, *Fellow, IEEE*

***Abstract*—A novel equivalent circuit for pulsed photoconductive sources is introduced for describing the coupling between the photoconductive gap and the antenna. The proposed circuit effectively describes the mechanism of feeding the antenna by the semiconductor when this latter is illuminated by a laser operating in a pulsed mode. Starting from the classical continuity equation, which models the free carriers density with respect to the laser power pump and the semiconductor features, a Norton equivalent circuit in the frequency-domain is derived. According to the Norton's theorem, the equivalent source representation is decoupled from the antenna. In particular, for photoconductive antennas, the Norton circuit takes into account of the electrical and optical properties of the semiconductor material, the features of the laser excitation, as well as the geometrical dimensions of the gap. The presence of the electrodes around the gap is part of the antenna and, therefore, it is taken into account in the antenna impedance. The proposed circuit allows the analysis of the coupling between the photoconductive source and the antenna, providing a tool to analyze and design photoconductive antennas.**

***Index Terms*—Equivalent circuit, photoconductivity, THz photoconductive antenna, THz radiated power, THz source, THz technology.**

I. Introduction

In recent years, Terahertz (THz) technology has attracted the interest of researchers for its variety of applications [1]–[15]. The emergence of all these applications has been driven by the availability of photoconductive antennas (PCAs), which have made available bandwidth in the THz spectrum at relatively low cost [1]–[4], [16]–[28].

In photoconductive antennas the basic mechanism for the THz power generation and detection relies on semiconductor materials pumped by laser. Specifically, when a laser source impinges on a semiconductor with an appropriate carrier frequency, it provides the required energy for the electrons to move from the valence band to the conduction band, and free electron-hole pairs are generated. The presence of free carrier pairs produces a change of the conductivity of the material, which becomes a photoconductor. The laser pump source typically operates in two different modes; i.e., Continuous Wave (CW) mode [1], [21] or Pulsed Wave (PW) mode [1], [16], [17]. The conductivity of the semiconductor material changes periodically in time according to the laser operating mode and the lifetime of the carriers in the semiconductor. Applying a biasing voltage (in transmission), inducing an electric field across the semiconductor gap, or impinging with THz radiation (in detection), these free charges are accelerated. A time-varying current is induced across the photoconductive gap, because of the acceleration of the free carriers. This effect is clearly localized on the gap, however it induces a global propagation of electromagnetic fields in the surrounding of the antenna structure. The propagating signal has frequency components that depend on the modulating signal of the laser pump and the semiconductor response to the laser excitation, as well as the geometrical features of the structures connected to the electrodes. Some frequencies will be more or less excited depending on the frequency response characterizing the surrounding structures.

The maximum available power of a single PCA in transmission is limited by the number of charges that can be excited to the conduction band of the semiconductor, by their mean velocity, by the coupling of the current in the gap with the surrounding antenna structure, and by the thermal failure of the device [18], [21].

In order to take into account all these aspects, in recent years different hybrid equivalent circuits have been developed for both the CW [1], [21], [24] and the PW operating mode [22], [25], [27], [28]. However, for PW mode, none of them constitutes a frequency-domain equivalent Thévenin or Norton circuit [29] representative of the THz radiation, because of the simultaneous presence of biasing and THz components in such circuits. Without decoupling the antenna from the source, these circuits associate a conductance and a capacitance (due to the presence of the electrodes) to the current source. According to the Thévenin and Norton theorems, such capacitive load is, instead, part of the antenna impedance. In fact, only in dipole like antennas the capacitive loading of the antenna gap is the dominant contribution to the reactive energy localized closed to the gap. Assuming a capacitive contribution, as part of the source, can be misleading in slot based designs, where the reactive loading close to the gap is mostly inductive [30]. In this work we propose a simple and effective Norton equivalent

Manuscript received Month DD, YYYY; revised Month DD YYYY. First published Month DD, YYYY; current version published Month DD, YYYY. This work was supported by the European Research Council Starting Grant ERC-2011-StG Grant AAATSI, No. 278794.

The authors are with the Microelectronics department of the Electrical Engineering, Mathemathics and Computer Science Faculty, Delft University of Technology, Mekelweg 4, 2628 CD Delft, The Netherlands (e-mail: a.garufo@tudelft.nl, g.carluccio@tudelft.nl, n.llombartjuan@tudelft.nl, a.neto@tudelft.nl).

Color versions of one or more of the figures in this paper are available online at http://ieeexplore.ieee.org.

Digital Object Identifier XX.XXXX/TAP.XXXX.XXXXXXXX.

model for PW operating mode, which takes into account of all the optical, electrical, and geometrical parameters of the photoconductive generator. It is, therefore, useful for describing the coupling between the photoconductive feed and the radiating antenna. A validation of the proposed equivalent circuit via power and spectrum measurements of some PCA prototypes will be shown in [31].

The paper is structured as follows: Section II is devoted to the description of the frequency-domain equivalent Norton circuit derivation from the time-domain circuit representation of the PCAs; Section III shows the use of the proposed frequency-domain equivalent Norton circuit to estimate the energy spectral density and the relevant average power radiated by the photoconductive antenna along with some numerical results for three different antenna structures. Section IV contains some concluding remarks. Finally, Appendix A describes some details about the modelling of the pulsed laser beam, which illuminates the semiconductor; Appendix B reports the model used for describing the photo-generation and recombination of carriers in the semiconductor gap; whereas Appendix C is dedicated to the derivation of the expression of the time-varying conductance of the semiconductor gap, when it is illuminated by the laser power pump.

II. Equivalent Norton Circuit Model for Photoconductive Sources

A photoconductive antenna is an optoelectronic device which is used to emit and receive electromagnetic energy in the THz frequencies bandwidth. It is typically obtained by placing thin metallizations around a slab of photoconducting material which is illuminated by a laser beam $\mathbf{s}_{laser}(\mathbf{r};t)$, as it is shown in Fig. 1(a). The performances of such device are affected by various phenomena, i.e., the interaction between the laser source and the semiconductor, the geometrical parameters of the active gap which feeds the antenna, and the electromagnetic radiative properties of the entire structure. In order to take into account all these aspects, different equivalent circuit models have been proposed in [1], [21], [22], [24], [25], [27], [28] by using different approximations. However, until now, there is no theoretical model in terms of an equivalent frequency-domain Thévenin or Norton circuit [29], which takes into account of the frequency behaviour of both the current distributions in the excited photoconductive area and the coupling to the antenna for PW mode. Thévenin and Norton equivalent circuits are the classical tools used in electronic engineering for quantifying and maximizing the power radiated by an antenna [29]. The absence of such model makes the investigation of the impedance matching between the photoconductive source and the antenna very difficult. In this work we propose a novel Norton equivalent circuit for modelling the PCA feeding mechanism. In the model we assume that the photoconductive gap dimensions of the antenna, Fig. 1(a), are small in terms of the wavelength (the wavelength relevant to the highest frequency of the pulse bandwidth in PW mode). In the model we also assume that the laser spot dimension is comparable or bigger than the gap size, in order to get a reasonable uniform illumination of the gap. Saturation effects due to high level of laser fluence on the gap are not considered [32], and moreover the screening effects due to the space–charge screening [22], and due to radiation field screening [32] are also neglected.

A. Time-Domain Circuit Representation

A schematic representation of a generic PCA is depicted in Fig. 1(a). The antenna is connected to a biasing voltage and its input terminals to the photoconductive material.

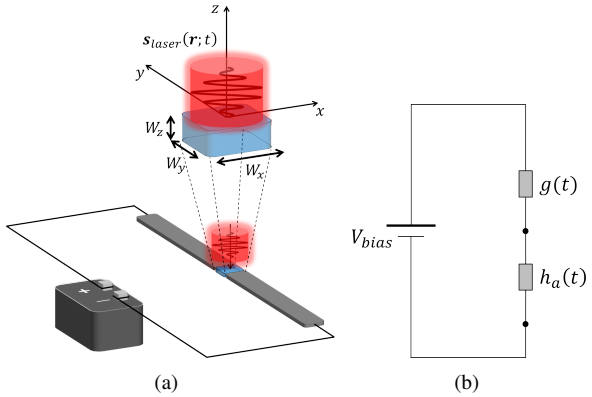

Figure 1. a) Photoconductive antenna schematic representation. The inset shows the photoconductive antenna gap. b) Photoconductive antenna time-domain circuit representation.

The photoconductor volume with dimensions (W_x, W_y, W_z) in the gap between the terminals is excited by a modulating laser with an intensity distribution $\mathbf{s}_{laser}(\mathbf{r};t)$, which is modelled as discussed in Appendix A. The laser pulse provides the energy to free the electrons in the semiconductor material, thus changing the conductivity of the photoconductor gap as discussed in Appendix B. As a result, the time-varying conductivity is expressed as:

$$\sigma(\mathbf{r};t) = e\,\mu\left(1-|\Gamma|^2\right)\frac{1-e^{-\alpha W_z}}{W_z} h(t) \otimes \left|\tilde{\mathbf{s}}(\boldsymbol{r};t)\right|_{z=0} \quad (1)$$

for $-W_z \leq z \leq 0$, where e is the elementary charge; μ is the free carriers transient mobility; Γ is the optical Fresnel reflection coefficient at the air-semiconductor interface; α is the laser absorption coefficient of the semiconductor material.

The time-varying conductivity (1) depends on the time convolution $\otimes$, as defined in (C.7), between the envelope of the laser power density $\tilde{\mathbf{s}}(\boldsymbol{r};t)$, and the impulsive response of the material $h(t)$ with respect to the laser power excitation [21], obtained as the Inverse Fourier Transform of (B.6):

$$h(t) = IFT\left[H(\omega)\right] = \frac{1}{hf_g}\, e^{-\frac{t}{\tau}} u(t) \quad (2)$$

where h is the Planck's constant; f_g is the frequency associated to the energy band-gap $E_g = hf_g$ of the semiconductor material; τ is the charge carrier lifetime; and $u(t)$ is the Heaviside step function. This schematic representation can be depicted as the circuit in Fig. 1(b), with concentrated quantities, discussed in Appendix C, rather than the distributed quantities described in Appendix B.

Specifically, the circuit is composed by three components.

The first one is the bias voltage V_{bias}. The second one is a time-varying conductance $g(t)$, representing the electrical properties of the gap, expressed by (C.6) in Appendix C:

$$g(t) = \eta(W_x, W_y, W_z, A_{laser}) \frac{A_{laser}}{W_y^2} e\,\mu\,h(t) \otimes \tilde{s}(t) \quad (3)$$

where A_{laser} is the area of the spatial distribution of the laser beam Poynting vector at the semiconductor interface, as defined in (A.8), and η is the laser absorption efficiency defined in (C.8). All the parameters present in equations (1)–(3) are discussed in detail in Appendixes A–C. Finally, the third component of the circuit is an impulsive response $h_a(t)$, representing the antenna in time-domain. The impulse response is depicted in series, since its current is the same current as that which flows through the gap. In a time-domain analysis, the evaluation of the field radiated by the antenna typically involves a time convolution integral, which depends on the geometry and the antenna radiation mechanism. However, this time-domain approach is not suitable for analyzing the spectral behavior of the antenna. To avoid such problem, antennas are typically studied in frequency-domain and are characterized by means of an impedance $Z_a(\omega)$ in circuit model.

B. Frequency-Domain Norton Circuit Model for Photoconductive Source

In order to study the coupling between the photoconductor gap and the antenna, it is useful to use an equivalent Norton circuit. Norton's theorem states that, in the frequency-domain the current flowing in a load at the terminals of a complex linear electrical system can be obtained by replacing the entire system with only two equivalent components: an equivalent current generator and an equivalent impedance, which provides a representation of the complex circuit completely decoupled from the load. Indeed, for PW mode, the proposed circuit differs to the ones proposed in the literature [24], [27], since it does not present a capacitive loading as part of the source which, according to the Norton's theorem, is part of the reactive antenna load and, moreover, it is not always capacitive as in case of long slots [30]. Fig. 2(a) presents such equivalent circuit, when the load is assumed to be the antenna under analysis.

The Norton equivalent frequency-domain current generator requires the evaluation of the spectrum of the current generator $I_g(\omega)$ flowing at the terminals of the antenna, when the antenna itself is short-circuited, as in Fig. 2(b). Considering that the gap dimensions are small in terms of the wavelength and they are comparable with the laser spot size, the field contributions due to the electron and hole local separation mechanism and to the electrodes scattering do not significantly change the applied bias field intensity [22], [42], and the total electric field in the volume of the gap can be approximated with the applied bias electric field $\mathbf{e}(\mathbf{r};t) \approx -V_{bias}/W_y\hat{\mathbf{y}}$. Consequently, the short-circuit current flowing across the gap, according to (C.4), is defined as $i_g(t) \approx g(t)\,V_{bias}$ and its spectrum is obtained simply performing the FT of the time-domain current derived by the time-domain description, i.e.:

$$I_g(\omega) = FT[i_g(t)] \quad (4)$$

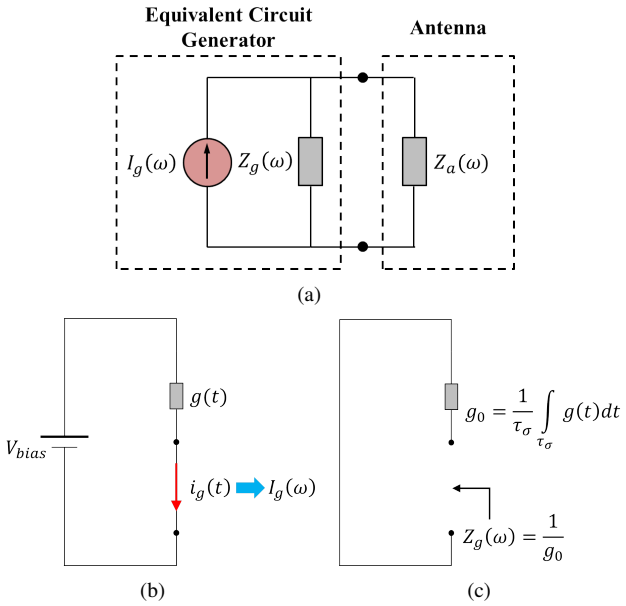

Figure 2. a) Equivalent Norton frequency-domain circuit. Schematic derivation for b) the equivalent generator current, and c) the equivalent generator impedance.

By using (C.4) and (C.5) in (4):

$$I_g(\omega) = \eta(W_x, W_y, W_z, A_{laser}) \cdot \cdot \frac{A_{laser}}{W_y^2} e\,\mu\,H(\omega)\,\tilde{S}(\omega)\,V_{bias} \quad (5)$$

Note that $i_g(t)$ well approximates the current flowing in the photoconductive gap in absence of the antenna, when the gap is small and illuminated with laser beams with diameter comparable or bigger than the gap size, as discussed in [42].

The equivalent Norton generator impedance is the impedance $Z_g(\omega)$ exhibited at the antenna terminals, in absence of the antenna, as in Fig. 2(c), for each frequency, when the bias voltage generator is removed. From the circuit, it is evident that it represents the impedance at the terminals of the photoconductor gap. However, $Z_g(\omega)$ is not the FT of the time-varying resistance, but it is the ratio of voltage and current spectra at the terminals for each frequency:

$$Z_g(\omega) = \frac{V(\omega)}{I(\omega)} \quad (6)$$

Since one has no easy way to evaluate (6), due to the various physical phenomena involved in the photoconductor when it is illuminated by a laser beam [41], we introduce a zero-th order approximation considering to have a constant conductance $g(t)$, when the photoconductor is illuminated, and that at each frequency the relation between the voltage and the current spectra in the photoconductor is real. In detail, the equivalent Norton generator impedance can be approximated as the inverse of the average conductance g_0 of the time-varying conductance $g(t)$ (Fig. 2(c)) on the time interval τ_σ where the conductivity of the gap is different from zero:

$$Z_g(\omega) \approx r_0 = \frac{1}{g_0} = \frac{1}{\frac{1}{\tau_\sigma}\int_{\tau_\sigma} g(t)\,\mathrm{d}t} \quad (7)$$

By using (C.6) and the results in Appendixes A–C, the average conductance is:

$$g_0 = \eta\left(W_x, W_y, W_z, A_{laser}\right) \cdot \cdot \frac{A_{laser}}{W_y^2} e\,\mu\,\frac{1}{\tau_\sigma} H\left(\omega = 0\right)\tilde{S}\left(\omega = 0\right) \quad (8)$$

It is worth noting that in (8), for the PW mode τ_σ defines a reasonable time interval in which one can do an average of the time-varying conductance pulse. In the results discussed in this work, τ_σ is the time duration of the pulsed conductivity, defined as the time interval where the conductivity is above one hundredth of its peak value as it is shown in Fig. 3(a). The chosen value guarantees an interval sufficiently long for considering the entire pulse and, at the same time, not too long to consider a time range where the conductance is ideally zero, Fig. 3(a). This time interval constitutes the time range in which the antenna is effectively excited and, consequently, for estimating the mean value of the equivalent generator impedance. Therefore, the mean resistance r_0 depends on the mean number of carriers which are in the conduction band of the photoconductor during the pulse duration in the PW operating mode. For such devices, most of the energy is contained at the lower frequencies of the spectrum. Therefore, the time average value of the conductance is a reasonable approximation since, for gaps smaller than the wavelength, the reactive part of the generator impedance is negligible. At higher frequencies, for electrically larger gaps, a complex impedance would describe better the behavior of the photoconductor. However, the amount of energy available at such frequencies is anyway smaller.

As an example, the values of the photoconductor time-varying conductance (3), and the relevant mean values (8) are reported in Fig. 3(a), considering a photoconductor volume of thickness $2\,\mu$m; an absorption coefficient $\alpha = 10^6\,\mathrm{m}^{-1}$; a carrier lifetime $\tau = 0.3\,$ps; and a carriers transient mobility $\mu = 300\,\mathrm{cm}^2/\mathrm{Vs}$ [32]–[34]. The results refer to a Gaussian laser beam profile with diameter at $-3\,$dB equal to the size of the gap surface $D_{laser} = W_x = W_y$; a carrier frequency $f_{laser} = 375\,$THz (central wavelength $\lambda_{laser} = 800\,$nm), a pulse repetition rate $f_p = 80\,$MHz; a half-power pulse width $\tau_p = 100\,$fs; and an average power $\bar{P}_{laser} = 30\,$mW.

The time-varying resistance $r\left(t\right)$ and its time average r_0 on the time interval τ_σ, which are the reciprocal of (3) and (8), respectively, are plotted in Fig. 3(b). As it is shown, when the photoconductor is not excited by the laser, the equivalent Norton resistance assumes extremely high values, which depends on the intrinsic free carrier concentration in the photoconductor. On the contrary, when the photoconductor is optically excited, it is theoretically possible to realize a matching between the equivalent Norton generator and the antenna.

Finally, as it is shown in Fig. 4, for a fixed gap size and laser energy, the laser beam focusing on the gap is crucial to achieve the impedance matching condition between the photoconductive source and the antenna impedance. Indeed, the generator resistance increases as the laser beam diameter increases compared to the area of the gap; i.e., focusing the laser power on a smaller area decreases the resistance of the photoconductor, as it is expected by (8). By decreasing the size of the laser beam, more laser power is absorbed by the photoconductor material and the resistance value decreases up to where the laser beam illuminates homogeneously the entire photoconductor gap area. The range of validity of these results has been validated when the laser beam waist is comparable or bigger than the gap area [31].

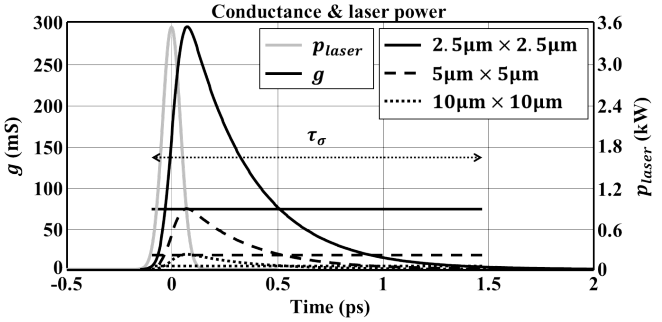

(a)

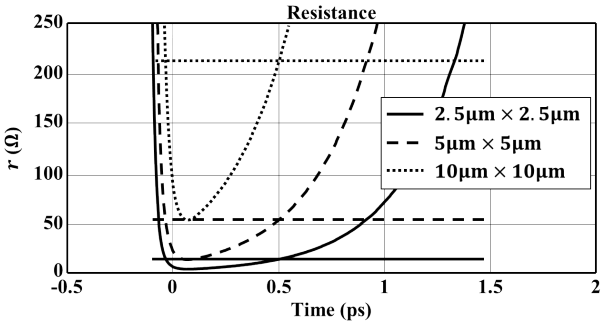

(b)

Figure 3. Time-dependency of the generator a) conductance and its related b) resistance of the photoconductor material illuminated by a laser operating in PW mode. The laser beam, with average power $\bar{P}_{laser} = 30\,$mW, is focused on different gap sizes. The solid light gray line in a) represents the time-varying pulse power envelope of the laser beam. The laser beam diameter at $-3\,$dB is focused on three different gap areas: $10\,\mu\mathrm{m} \times 10\,\mu\mathrm{m}$ (black dotted line); $5\,\mu\mathrm{m} \times 5\,\mu\mathrm{m}$ (black dashed line); and $2.5\,\mu\mathrm{m} \times 2.5\,\mu\mathrm{m}$ (black solid line). The straight horizontal lines refer to the related mean values during the pulse duration τ_σ.

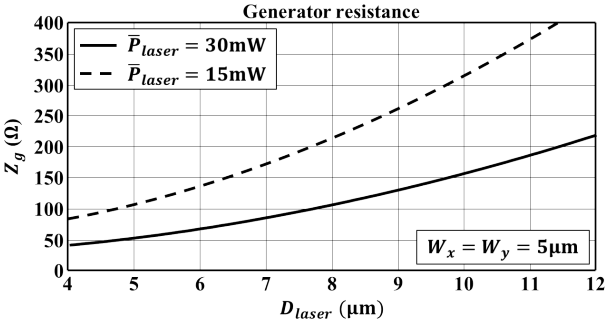

Figure 4. Laser beam diameter dependency of the generator resistance of a photoconductor material illuminated by a laser operating in PW mode.

III. Radiated Energy Spectral Density and Average Power

The evaluation of the energy spectral density and the average power radiated by the PCA is shown in this section. They are calculated from the equivalent circuit model proposed in Section II-B.

By supposing a finite energy voltage signal $v(t)$ and its related current signal $i(t)$, it is possible to derive the instantaneous power $p(t) = v(t)\, i(t)$ and the energy E of the signal, which can be evaluated also knowing the spectra of the voltage and current, resorting to the generalized Parseval's theorem [43]:

$$E = \int_{-\infty}^{+\infty} v(t)\, i(t)\, \mathrm{d}t = \frac{1}{2\pi} \int_{-\infty}^{+\infty} V(\omega)\, I^*(\omega)\, \mathrm{d}\omega \quad (9)$$

where $V(\omega) = FT[v(t)]$ and $I(\omega) = FT[i(t)]$ are the spectra of the voltage and current signals, respectively. The product of the voltage spectrum $V(\omega)$ and the conjugate current spectrum $I(\omega)$ in (9) represents the energy spectral density associated with the voltage $v(t)$ and current $i(t)$ signals.

Referring to the Norton equivalent circuit in Fig. 2(a), by using formulas (5) and (7), one can calculate the spectrum of the current generator $I_g(\omega)$ and the generator impedance $Z_g(\omega)$ of the photoconductor, respectively. Given the antenna impedance $Z_a(\omega)$, which can be estimated by using analytical formulas or by numerical tools, the spectrum of the current $I_a(\omega)$, flowing in the antenna load, can be easily evaluated. By knowing the spectrum of the current flowing into the antenna load $I_a(\omega)$ and the antenna impedance $Z_a(\omega)$, it is possible to derive the energy spectral density associated with the antenna radiation:

$$E_s(\omega) = V_a(\omega)\, I_a^*(\omega) = \\ = Z_a(\omega) \left| \frac{Z_g(\omega)}{Z_a(\omega) + Z_g(\omega)} \right|^2 |I_g(\omega)|^2 \quad (10)$$

The energy generated by the PCA can be evaluated by integrating (10), using relation (9):

$$E_{source} = \frac{1}{2\pi} \int_{-\infty}^{+\infty} E_s(\omega)\, \mathrm{d}\omega \quad (11)$$

The result of this integral is a real quantity, because of the Hermitian symmetry of the spectrum. Since the real part of the impedance in lossless antennas accounts for radiation, (11) provides the radiated energy in each pulse. Furthermore, since the PCA radiates pulses periodically with a period $T_p = 1/f_p$, where f_p is the repetition rate of the laser, the average power radiated by the antenna can be calculated as:

$$\bar{P}_{source} = \frac{E_{source}}{T_p} \quad (12)$$

Defining the matching efficiency η_m between the antenna and the photoconductive source as the ratio between the energy spectral density E_s radiated by the antenna and the energy spectral density E_s^{max} of the maximum available energy provided by the photoconductor gap to a matched load antenna, the energy spectral density E_s can be expressed also as:

$$E_s(\omega) = \eta_m(\omega)\, E_s^{max}(\omega) \quad (13)$$

The maximum available energy $E_{available}$ can thus be estimated as in (11), by integrating the energy spectral density E_s^{max}:

$$E_{available} = \frac{1}{2\pi} \int_{-\infty}^{+\infty} E_s^{max}(\omega)\, \mathrm{d}\omega \quad (14)$$

Therefore, taking into account that the pulses are periodically radiated with a repetition period T_p, the maximum available average power $\bar{P}_{availalble}$ can be evaluated as:

$$\bar{P}_{available} = \frac{E_{available}}{T_p} \quad (15)$$

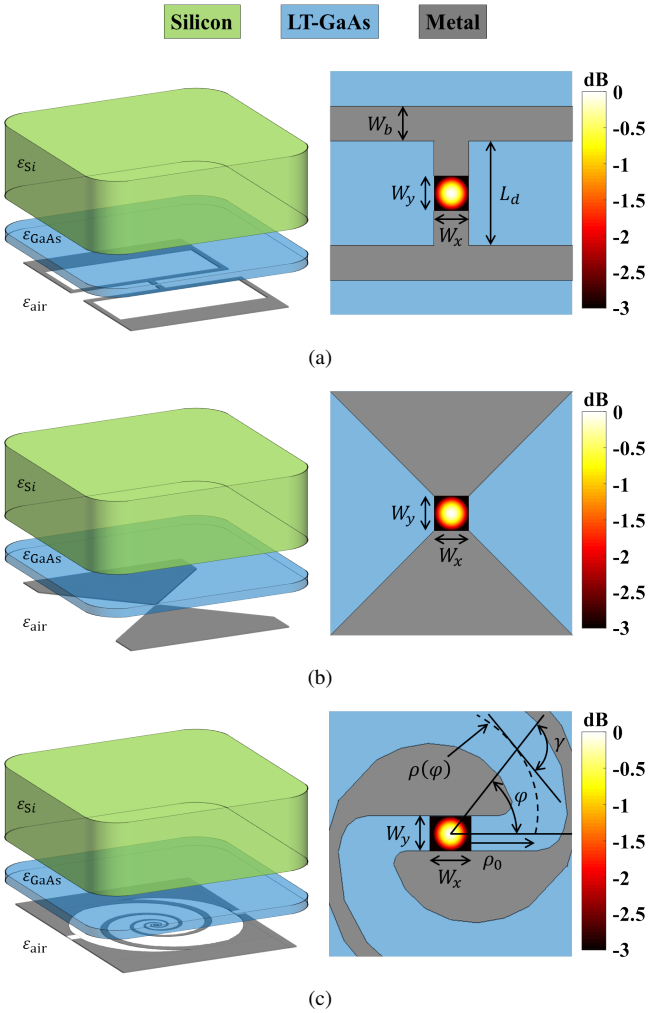

Figure 5. PCA geometries and structures: the blue slab represents the chip of photoconductive material; the green thick slab depicts the silicon semi-infinite medium; whereas the antenna metallizations are depicted in grey. a) H-dipole antenna: gap size $W_x = W_y = 10\,\mu$m, dipole length $L_d = 30\,\mu$m and bias lines width $W_b = 10\,\mu$m. b) Bow-tie antenna: gap size $W_x = W_y = 10\,\mu$m and tapering angle 90°. c) Logarithmic spiral antenna: $\rho(\varphi) = \rho_0 e^{a\varphi}$ with $\varphi \in [0, 2\pi N]$, starting radius $\rho_0 = 23\,\mu$m, curvature angle $\gamma = 76.5°$, winding number $N = 2.6$, tapering angle $\delta = 150°$ and gap width $W_y = 10\,\mu$m. In the zoom of the gap of each antenna, it is shown the normalized laser power density spatial distributions, $D_{laser} = 10\,\mu$m, used for the evaluation of the energy spectral density in Fig. 7.

As an example, we apply the above discussed analysis to three different antenna geometries, i.e., the H-dipole, the bow-tie, and the spiral antenna (Fig. 5), which are the most common geometries for PCA found in the literature, [1]–[4].

Table I
ESTIMATED GENERATOR IMPEDANCE Z_g, AVERAGE CURRENT $\tilde{I}_g$ OF A PULSE ON THE TIME INTERVAL τ_σ, AND AVAILABLE POWER $\bar{P}_{available}$ PROVIDED BY THE PHOTOCONDUCTOR GAP USING AN AVERAGE POWER OF THE LASER $\bar{P}_{laser} = 30\,\mathrm{mW}$, AND AN APPLIED BIAS ELECTRIC FIELD $E_{bias} = 4\,\mathrm{V}/\mu\mathrm{m}$.

Gap size	V_{bias} $(E_{bias} = 4\,\mathrm{V}/\mu\mathrm{m})$	D_{laser}	**Fluence**	Z_g	$\tilde{I}_g$	$\bar{P}_{available}$
$10\,\mu\mathrm{m} \times 10\,\mu\mathrm{m}$	$40\,\mathrm{V}$	$10\,\mu\mathrm{m}$	$0.21\,\mathrm{mJ/cm^2}$	$214\,\Omega$	$188\,\mathrm{mA}$	$469\,\mu\mathrm{W}$
$5\,\mu\mathrm{m} \times 5\,\mu\mathrm{m}$	$20\,\mathrm{V}$	$5\,\mu\mathrm{m}$	$0.87\,\mathrm{mJ/cm^2}$	$54\,\Omega$	$376\,\mathrm{mA}$	$469\,\mu\mathrm{W}$
$2.5\,\mu\mathrm{m} \times 2.5\,\mu\mathrm{m}$	$10\,\mathrm{V}$	$2.5\,\mu\mathrm{m}$	$3.47\,\mathrm{mJ/cm^2}$	$13\,\Omega$	$752\,\mathrm{mA}$	$469\,\mu\mathrm{W}$

The H-dipole and the bow-tie do not present any particular design features, and the logarithmic spiral has been designed according to [44] with the limitation of designing a gap with length $W_y = 10\,\mu\mathrm{m}$. The geometrical features of the antennas are listed in the caption of Fig. 5. The maximum sizes of the antennas are the same for all the three geometries $3\,\mathrm{mm} \times 2\,\mathrm{mm}$. The layered structure is the same for all the antennas: the antenna metallization is placed on a slab of $2\,\mu\mathrm{m}$ Low-Temperature-grown Gallium Arsenide (LT-GaAs), which is grown on a Semi-Insulating Gallium Arsenide (SI-GaAs) wafer, $525\,\mu\mathrm{m}$ thick with $\varepsilon_{\mathrm{GaAs}} = 13$ (typical size and permittivity of a GaAs substrate used for PCAs). The antenna chip has been simulated by the EM commercial software [45], by considering the structure radiating between free space and a semi-infinite dense dielectric with $\varepsilon_{\mathrm{Si}} = 11.9$, in order to approximate the effect of the presence of a silicon dielectric lens [46], typically used for such kind of devices for enhancing the directivity of the antenna.

The simulated input impedances are shown in Fig. 6, whereas the energy spectral densities radiated by the antennas are shown in Fig. 7, considering the same laser beam features and optical and electrical parameters of the photoconductor listed in Section II-B. Referring to Fig. 5, the following sizes of the gap area illuminated by the laser beam for the three geometries have been considered: $W_x = W_y = 10\,\mu\mathrm{m}$ for the H-dipole and the bow-tie antenna, while $W_x = 12\,\mu\mathrm{m}$ and $W_y = 10\,\mu\mathrm{m}$ for the logarithmic spiral antenna due to the geometry of its gap.

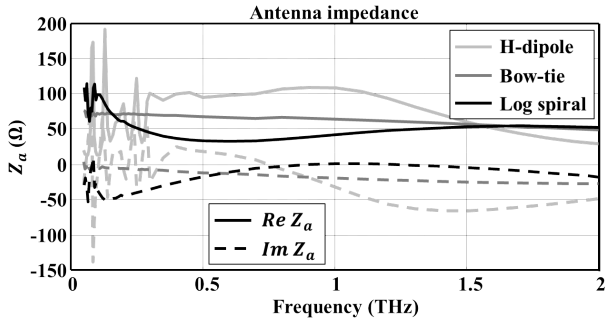

Figure 6. Simulated input impedances of the antenna geometries under analysis.

It is noted that the photoconductor generator is mismatched under such working conditions, providing a generator impedance $Z_g = 214\,\Omega$ for the H-dipole and bow-tie antennas, and $Z_g = 193\,\Omega$ for the logarithmic spiral. The energy spectral densities radiated by the antennas present almost the same behavior at the higher frequencies of the spectrum. Significant differences can be noticed at the lower frequencies where they show different behaviours due to the finiteness of the different geometries, which results in different resonance behaviours. The average power $\bar{P}_{source}$ generated by the antennas is practically the same: $342\,\mu\mathrm{W}$, $339\,\mu\mathrm{W}$, and $326\,\mu\mathrm{W}$ for the H-dipole, bow-tie, and logarithmic spiral, respectively. For

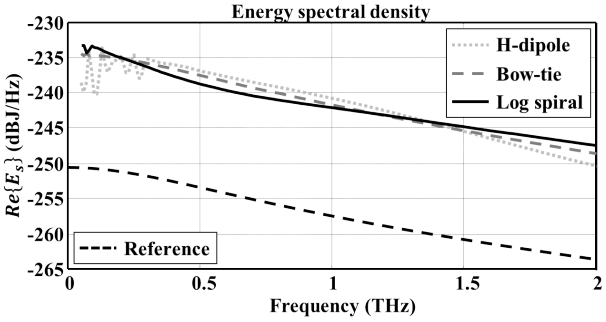

Figure 7. Simulated energy spectral densities E_s generated by the three antennas under analysis. The black dashed line is the reference energy spectral density, generated by the equivalent current generator $I_g(\omega)$ of the antennas, connected to a reference load $R = 1\,\Omega$.

sake of completeness, the reference energy spectral density, evaluated considering the equivalent current generator of the antennas connected to a reference load $R = 1\,\Omega$ at each frequency is also shown in Fig. 7.

It is worth noting that, referring to Table I, the power $\bar{P}_{source}$ estimated for the antennas in the previous numerical example, does not constitute the maximum available power, because of the impedance mismatch between the photoconductor equivalent circuit and the antenna impedance. Indeed, a gap with the same size $W_x = W_y = 10\,\mu\mathrm{m}$, illuminated by the same average laser power $\bar{P}_{laser} = 30\,\mathrm{mW}$, and same applied bias voltage $V_{bias} = 40\,\mathrm{V}$, provides a higher available power $\bar{P}_{available}$, if it is ideally connected to a matched antenna load at each frequency, as it is shown in the second row of Table I. Moreover, in Table I it is shown that focusing the same laser power on smaller gap, and keeping the same applied bias electric field on the gap, $E_{bias} \simeq V_{bias}/W_y$ (second column), does not change the maximum available power $\bar{P}_{available}$ provided by the source. Indeed, by focusing the laser beam on smaller gaps (columns one, three, and four in Table I), the impedance of the equivalent generator decreases (fifth column in Table I), whereas the current of the equivalent generator increases. In the sixth column of Table I, we report the average current $\tilde{I}_g$ of the pulse on the time interval τ_σ. The resulting available power $\bar{P}_{available}$ for all the gap sizes is shown in the

last column of Table I.

A complete analysis of the energy spectral densities and power radiated by the photoconductive antennas, together with a validation of the proposed equivalent circuit via power measurements of some prototypes, will be shown and discussed in detail in the separate work [31].

IV. Conclusion

In this work a novel frequency-domain Norton equivalent circuit model has been proposed to characterize the source of pulsed photoconductive antennas. The model takes into account the properties of the semiconductor material, the geometrical parameters of the source, and the laser excitation involved. The presence of the electrodes around the photoconductive gap is taken into account in the antenna impedance, thus decoupling the photoconductive source from the antenna. The equivalent circuit can be used to evaluate the energy spectral density and the average power radiated by a PCA. The model clarifies that the power generated and radiated by commonly used photoconductive antennas can be of the order of some hundreds of microwatts. Instead, how much power can be used depends on the quasi optical coupling to the receiver. This aspect will be addressed in the second part of these sequence of papers, jointly with an experimental validation. Therefore, the proposed equivalent circuit provides an effective tool to design and analyze PCAs, since it can be used to estimate and maximize the power radiated by PCAs.

Appendix A
Pulsed Laser Source Model

A typical laser source used to generate electron-hole pairs in photoconductor is characterized by a spectral band (large for pulsed systems and small for continuous wave systems) centered around a laser carrier frequency (e.g. $f_{laser} = 375\,\mathrm{THz}$ for LT-GaAs).

Considering the pulsed laser as a paraxial wave modulated by slowing-varying pulses, which means that the envelope of the pulse is relatively constant within a laser cycle, because of the narrow bandwidth, $B_{laser} \ll f_{laser}$, the spatial behavior is approximately the same as that of a monochromatic wave at frequency f_{laser} (CW laser) and it can be regarded as quasi-CW pulse wave. Referring to the coordinate system in Fig. 1(a), the laser electric field can be expressed as [50]:

$$\mathbf{e}\left(\mathbf{r};t\right) = \mathbf{e}_0\left(\boldsymbol{\rho},z\right) f\left(t-\frac{z}{c}\right)\cos\left(\omega_{laser}t - k_{laser}z + \varphi_{laser}\right) \tag{A.1}$$

where $f\left(t\right)$ is the periodic laser modulating signal, which can be expressed as:

$$f\left(t\right) = \sum_{i=-\infty}^{+\infty} \tilde{f}\left(t-\frac{z}{c}-iT_p\right) \tag{A.2}$$

where $\tilde{f}$ is the base band function defined on one period T_p of the laser pulse repetition rate. Moreover, in (A.1) $\mathbf{e}_0\left(\boldsymbol{\rho},z\right) = E_0\mathbf{e}_n\left(\boldsymbol{\rho},z\right)$ is the transverse spatial distribution of the beam electric field, E_0 is the peak amplitude of the electric field, and $\mathbf{e}_n\left(\boldsymbol{\rho},z\right)$ is the spatial distribution of the electric field with unitary amplitude, which is also function of z due to the diffraction effect of the laser beam. By considering only a single pulse of the laser, the EM power per unit area transported by such a wave is represented as a function of the electric and magnetic fields by using the Poynting vector:

$$\mathbf{s}\left(\mathbf{r};t\right) = \mathbf{e}\left(\mathbf{r};t\right)\times\mathbf{h}\left(\mathbf{r};t\right) \tag{A.3}$$

Defining the pulse time envelope of the Poynting vector as:

$$\tilde{s}_n\left(t-\frac{z}{c}\right) = \left|f\left(t-\frac{z}{c}\right)\right|^2 \tag{A.4}$$

The expression (A.3) can be written as:

$$\mathbf{s}\left(\mathbf{r};t\right) = \frac{1}{\zeta}\left|\mathbf{e}_0\left(\boldsymbol{\rho},z\right)\right|^2\tilde{s}_n\left(t-\frac{z}{c}\right)\cdot \\ \cdot\cos^2\left(\omega_{laser}t - k_{laser}z + \varphi_{laser}\right)\left(-\hat{\mathbf{z}}\right) \tag{A.5}$$

Considering that the envelope of the electromagnetic pulse is relatively constant within a laser period, one can calculate the average on the laser period $T_{laser} = 1/f_{laser}$ of the density power carried each second by the pulse:

$$\tilde{\mathbf{s}}\left(\mathbf{r};t\right) = \frac{1}{T_{laser}}\int_{nT_{laser}}^{(n+1)T_{laser}}\mathbf{s}\left(\mathbf{r};t\right)\mathrm{d}\tau \\ = \frac{1}{2\zeta}\left|\mathbf{e}_0\left(\boldsymbol{\rho},z\right)\right|^2\tilde{s}_n\left(t-\frac{z}{c}\right)\left(-\hat{\mathbf{z}}\right) \tag{A.6}$$

Defining the spatial distribution of the Poynting vector as:

$$\tilde{\mathbf{s}}\left(\boldsymbol{\rho},z\right) = \frac{1}{2\zeta}\left|\mathbf{e}_0\left(\boldsymbol{\rho},z\right)\right|^2 = S_0\left(z\right)\tilde{\mathbf{s}}_n\left(\boldsymbol{\rho},z\right) \tag{A.7}$$

where $S_0\left(z\right) = P_0/A_{laser}\left(z\right)$ is the peak amplitude of the pulse envelope of the Poynting vector in z, which is related to the peak power of the pulse P_0; and $\tilde{\mathbf{s}}_n\left(\boldsymbol{\rho},z\right)$ is the spatial distribution of the Poynting vector with unitary amplitude.

$$A_{laser}\left(z\right) = \int_{-\infty}^{+\infty}\int_{-\infty}^{+\infty}\tilde{\mathbf{s}}_n\left(\boldsymbol{\rho},z\right)\cdot\hat{\mathbf{z}}\,\mathrm{d}x\,\mathrm{d}y \tag{A.8}$$

is the area of the spatial distribution of the laser beam Poynting vector in z. The average power density carried by a laser pulse can be expressed as:

$$\tilde{\mathbf{s}}\left(\mathbf{r};t\right) = S_0\left(z\right)\tilde{\mathbf{s}}_n\left(\boldsymbol{\rho},z\right)\tilde{s}_n\left(t-\frac{z}{c}\right) \tag{A.9}$$

The remaining temporal dependence is associated with the modulating signal, $\tilde{s}_n\left(t\right)$. Assuming that the EM pulse travels along the negative z-direction, the average power carried each second by the EM pulse over a plane orthogonal to z is defined as:

$$p_{laser}\left(z;t\right) = \int_{-\infty}^{+\infty}\int_{-\infty}^{+\infty}\tilde{\mathbf{s}}\left(\boldsymbol{\rho},z;t\right)\cdot\left(-\hat{\mathbf{z}}\right)\mathrm{d}x\,\mathrm{d}y \\ = P_0\tilde{s}_n\left(t-\frac{z}{c}\right) \tag{A.10}$$

where P_0 is the peak power of the time-varying envelope of the pulsed signal with unitary amplitude $\tilde{s}_n\left(t\right)$.

By neglecting phase delay terms and assuming that $\tilde{s}_n\left(t\right)$ has the Gaussian shape:

$$\tilde{s}_n\left(t\right) = e^{-4\ln 2\frac{t^2}{\tau_p^2}} \tag{A.11}$$

where τ_p is the full width at half maximum (FWHM) duration of the pulse, with $\tau_p \ll T_p$, one can relate the peak power of the pulse P_0 with the laser average power $\bar{P}_{laser}$ by the relation:

$$E_p = \sqrt{\frac{\pi}{4\ln 2}} P_0 \tau_p = \bar{P}_{laser} T_p \tag{A.12}$$

where E_p is the energy of a single laser pulse. Assuming a given spatial transverse distribution (e.g., uniform, Gaussian, Airy pattern, etc.) for the laser electric field, and given a laser mean power $\bar{P}_{laser}$, from (A.9)–(A.12) one can derive the amplitude $S_0(z)$ of the Poynting vector $\tilde{\mathbf{s}}(\mathbf{r};t)$ and the amplitude of the laser electric field $\mathbf{e}(\mathbf{r};t)$.

Appendix B
Photoconductivity Model

In this appendix the expression for the conductivity of the volume of photoconductive material [1], [27], depicted in Fig. 1, when it is optically excited with the appropriate carrier frequency, is summarized for completeness and readability of the work. The conductivity of a photoconductor can be expressed in terms of the charge carrier density (electrons and holes) generated by an impinging electromagnetic wave. In order to explicitly derive an expression for the conductivity, one needs to calculate the charge concentration $n(\mathbf{r};t)$. Such concentration can be estimated by resorting to the semiconductor continuity equation [47], [48]:

$$\frac{\partial}{\partial t} n(\mathbf{r};t) = g_c(\mathbf{r};t) - r(\mathbf{r};t) \tag{B.1}$$

In (B.1), the term $g_c(\mathbf{r};t)$ is the carriers generation rate, whereas $r(\mathbf{r};t)$ is the carrier recombination rate, which can be expressed as:

$$r(\mathbf{r};t) = \frac{n(\mathbf{r};t)}{\tau} \tag{B.2}$$

where τ is the charge carrier lifetime. Here, the time τ is assumed to be the average value of the lifetimes for all the different kind of recombination phenomena in the photoconductor, according to the Matthiessen's rule [48]. In the semiconductor continuity equation (B.1) the carrier density at the thermal equilibrium is neglected, since it is typically negligible in presence of the optical pumping. Moreover, in (B.1) the diffusion term is also neglected, since the biasing is considered far dominant in inducing electric current across the investigated gap. Finally, we also neglect any spatial variation of the drift current, assuming negligible the spatial variation of the charges because of the almost uniform illumination of the gap, and assuming an approximately constant bias electric field across it. Therefore, in relation to the THz current generation, the dominant terms in the continuity equation (B.1) are the carriers generation $g_c(\mathbf{r};t)$ and recombination $r(\mathbf{r};t)$ terms.

The generation rate $g_c(\mathbf{r};t)$ is a function of the modulated laser signal impinging on the surface (W_x, W_y) of the photoconductor volume and it is proportional to the variation of the transmitted Poynting vector in the volume of the semiconductor material through the relation:

$$g_c(\mathbf{r};t) = -\frac{1}{hf_g}\frac{\mathrm{d}}{\mathrm{d}z}\left[\left(1-|\Gamma|^2\right)\tilde{\mathbf{s}}(\boldsymbol{\rho}, z=0;t)\, e^{-\alpha|z|}\right]\cdot\hat{\boldsymbol{z}} \tag{B.3}$$

where, $\tilde{\mathbf{s}}(\boldsymbol{\rho}, z=0;t)$ is the time-varying envelope of the Poynting vector distribution impressed by the laser source (Appendix A) evaluated at the interface between the air and the semiconductor and it only depends from the z-transverse vector $\boldsymbol{\rho}$; h is the Planck constant; f_g is the frequency associated with the energy band-gap $E_g = hf_g$, which separates the valence band from the conduction band in the crystal lattice of the photoconductor; α is the laser power absorption coefficient of the material; Γ is the optical Fresnel reflection coefficient at the air-semiconductor interface. In order to induce the electron band-to-band transitions in the photoconductor, the frequency of the carrier f_{laser} of the pulsed laser in the PW mode (or the two laser carrier frequencies in the CW mode) has to be greater than the band-gap frequency, i.e., $f_{laser} > f_g$. By using (A.9), the average generation rate along z can then be obtained as:

$$\begin{aligned}\bar{g}_c(\mathbf{r};t) =& \frac{1}{W_z}\int_{-W_z}^{0} g_c(\mathbf{r};t)\,\mathrm{d}z = \\ &= \left(1-|\Gamma|^2\right)\frac{1-e^{-\alpha W_z}}{W_z}\frac{1}{hf_g}\left|\tilde{\mathbf{s}}_n(\boldsymbol{\rho}, z=0)\right|\tilde{s}(t)\end{aligned} \tag{B.4}$$

with $-W_z \le z \le 0$. Using (B.2) and (B.4) in (B.1) and transforming (B.1) in the spectral domain with respect to the time, the equation can be solved as:

$$\begin{aligned}N(\mathbf{r};\omega) = \left(1-|\Gamma|^2\right)&\frac{1-e^{-\alpha W_z}}{W_z}\cdot \\ &\cdot\frac{1}{hf_g}\frac{\tau}{1+j\tau\omega}\left|\tilde{\mathbf{s}}_n(\boldsymbol{\rho}, z=0)\right|\tilde{S}(\omega)\end{aligned} \tag{B.5}$$

with $-W_z \le z \le 0$. From (B.5), one can define the frequency response to the laser excitation of the photoconductor material as:

$$H(\omega) = \frac{1}{hf_g}\frac{\tau}{1+j\tau\omega} \tag{B.6}$$

To evaluate the carriers density in the volume of the material $n(\mathbf{r};t)$, the Inverse Fourier Transform of (B.5) is applied. The time-varying conductivity in each point of the volume (W_x, W_y, W_z) due to the free carriers generated by the impinging laser power is evaluated as:

$$\sigma(\mathbf{r};t) = e\,\mu\, n(\mathbf{r};t) \tag{B.7}$$

where e is the elementary charge, and μ is the free carriers transient mobility of the photoconductor material.

Appendix C
Time-Varying Conductance of Photoconductor Source

This appendix summarizes, for completeness and for improving the readability of the paper, the derivation of the time-varying conductance $g(t)$ of the optically pumped photoconductor gap [27], depicted in Fig. 1(a).

By applying the Ohm's law, and assuming that the current impulse response to an applied electric field of the photoconductor is instantaneous [41], one obtains

$$\mathbf{j}(\mathbf{r};t) = \sigma(\mathbf{r};t)\,\mathbf{e}(\mathbf{r};t) \tag{C.1}$$

From (C.1), considering that the significant current is oriented along $\hat{\boldsymbol{y}}$ with reference to Fig. 1(a), the current flowing through the gap can be evaluated as:

$$i\left(t\right)=\frac{1}{W_y}\int_{-\frac{W_y}{2}}^{\frac{W_y}{2}}\int_{-\frac{W_x}{2}}^{\frac{W_x}{2}}\int_{-W_z}^{0}\mathbf{j}\left(\mathbf{r};t\right)\cdot\hat{\boldsymbol{y}}\,\mathrm{d}z\,\mathrm{d}x\,\mathrm{d}y \quad \text{(C.2)}$$

and the voltage drop as

$$v\left(t\right)=-\int_{-\frac{W_y}{2}}^{\frac{W_y}{2}}\mathbf{e}\left(\mathbf{r};t\right)\cdot\hat{\boldsymbol{y}}\,\mathrm{d}y\approx e_y\left(0;t\right)W_y \quad \text{(C.3)}$$

Therefore, the current flowing across the gap can be approximated as

$$i\left(t\right)\approx g\left(t\right)v\left(t\right) \quad \text{(C.4)}$$

where $g\left(t\right)$ is the time dependent conductance of the photoconductor gap:

$$g\left(t\right)=\frac{1}{W_y^2}\int_{-\frac{W_y}{2}}^{\frac{W_y}{2}}\int_{-\frac{W_x}{2}}^{\frac{W_x}{2}}\int_{-W_z}^{0}\sigma\left(\mathbf{r};t\right)\mathrm{d}z\,\mathrm{d}x\,\mathrm{d}y \quad \text{(C.5)}$$

As shown in [49], using the results in Appendix B, the time-varying conductance can be rewritten as:

$$g\left(t\right)=\eta\left(W_x,W_y,W_z,A_{laser}\right)\frac{A_{laser}}{W_y^2}e\,\mu\,h\left(t\right)\otimes\tilde{s}\left(t\right) \quad \text{(C.6)}$$

where $h\left(t\right)$ is the impulse response of the material with respect to the laser excitation defined as the Inverse Fourier Transform of (B.6), and $\otimes$ defines the time convolution integral as:

$$s\left(t\right)\otimes h\left(t\right)=\int_{-\infty}^{+\infty}s\left(t-\tau\right)h\left(\tau\right)\mathrm{d}\tau \quad \text{(C.7)}$$

In (C.6), the first term η quantifies the laser power absorption efficiency of the photoconductor gap, and it takes into account the spillover of the laser beam with respect to the photoconductor gap, the reflection at the interface air-photoconductor, and the laser power absorption property of the photoconductor:

$$\eta\left(W_x,W_y,W_z,A_{laser}\right)=\left(1-\left|\Gamma\right|^2\right)\frac{1-e^{-\alpha W_z}}{W_z}\cdot$$
$$\cdot\frac{1}{A_{laser}}\int_{-\frac{W_y}{2}}^{\frac{W_y}{2}}\int_{-\frac{W_x}{2}}^{\frac{W_x}{2}}\int_{-\frac{W_z}{2}}^{0}\left|\tilde{\mathbf{s}}_n\left(\boldsymbol{\rho};z=0\right)\right|\mathrm{d}z\,\mathrm{d}x\,\mathrm{d}y \quad \text{(C.8)}$$

where A_{laser} is the area of the spatial distribution with unitary amplitude of the laser beam Poynting vector at the photoconductor interface, as defined in Appendix A; $h\left(t\right)=IFT\left[H\left(\omega\right)\right]$ defines the impulsive response of the photoconductor material, and $\tilde{s}\left(t\right)$ is the time-varying envelope of the laser pulse.

ACKNOWLEDGMENT

The authors would like to thank the anonymous reviewers for their useful comments and their careful review of this paper.

REFERENCES

[1] D. Saeedkia, *Handbook of Terahertz Technology for Imaging, Sensing and Communication*, Cambridge, U.K., Woodhead, 2013.

[2] S. Preu, G. H. Dhler, S. Malzer, L. J. Wang, and A. C. Gossard, "Tunable, continuous-wave terahertz photomixer sources and applications," *J. Appl. Phys.*, vol. 109, 061301, Mar. 2011.

[3] P. U. Jepsen, D. G. Cooke, and M. Kock, "Terahertz spectroscopy and imaging–Modern techniques and applications," *Laser Photon. Rev.*, vol. 5, no. 1, pp. 124–166, Jan. 2011.

[4] M. Hangyo, M. Tani, T. Nagashima, H. Kitahara, and H. Sumikura, "Spectroscopy and imaging by laser excited terahertz waves," *Plasma and Fusion Research.*, vol. 2, S1020, 2007.

[5] M. Tonouchi, "Cutting-edge terahertz technology," *Nature Photon.*, vol. 1, pp. 97–105, Feb. 2007.

[6] D. G. Rowe, "Terahertz takes to the stage," *Nature Photon.*, vol. 1, pp. 75–97, Feb. 2007.

[7] J. F. Federici, B. Schulkin, F. Huang, D. Gary, R. Barat, F. Oliveira, and D. Zimdars, "THz imaging and sensing for security applications Explosives, weapons and drugs," *Semicond. Sci. Technol*, vol. 20, pp. S266–S280, July 2005.

[8] M. K. Choi, A. Bettermann, and D. W. Van Der Weide, "Potential for detection of explosive and biological hazards with electronic terahertz systems," *Philos. Trans. R. Soc. London A, Math. Phys. Sci.*, vol. 362, no. 1815, pp. 337–349, Feb. 2004.

[9] M. C. Kemp, P. F. Taday, B. E. Cole, J. A. Cluff, A. J. Fitzgerald, and W. R. Tribe, "Security applications of terahertz technology," *Proc. SPIE*, vol. 5070, pp. 44–52, Aug. 2003.

[10] P. Siegel, "Terahertz technology in biology and medicine," *IEEE Trans. Microw. Theory Techn.*, vol. 52, no. 10, pp. 2438–2447, Oct. 2004.

[11] P. F. Taday, "Applications of terahertz spectroscopy to pharmaceutical sciences," *Philos. Trans. R. Soc. London A, Math. Phys. Sci.*, vol. 362, no. 1815, pp. 351–364, Feb. 2004.

[12] T. Globus, D. Woolard, M. Bykhovskaia, B. Gelmont, L. Werbos, and A. Samuels, "THz-frequency spectroscopic sensing of DNA and related biological materials," *Int. J. High Speed Electron. Syst.*, vol. 13, no. 4, pp. 903–936, Dec. 2003.

[13] D. Mittleman, *Sensing with Terahertz Radiation.*, New York: Springer-Verlag, 2003.

[14] J. M. Bowen, "Towards terahertz communications Systems requirements," *Terahertz Sources and Systems*, Norwell, MA: Kluwer, pp. 269–283, 2001.

[15] D. Grischkowsky, S. Keiding, M. van Exter, and C. Fattinger, "Far-infrared time-domain spectroscopy with terahertz beams of dielectrics and semiconductors," *J. Opt. Soc. Am. B*, vol. 7, no. 10, pp. 2006–2015, Oct. 1990.

[16] D. H. Auston, K. P. Cheung, and P. R. Smith, "Picosecond photoconducting Hertzian dipoles," *Appl. Phys. Lett.*, vol. 45, no. 3, pp. 284–286, May 1984.

[17] P. U. Jepsen, R. H. Jacobsen, and S. R. Keiding, "Generation and detection of terahertz pulses from biased semiconductor antennas," *J. Opt. Soc. Am. B*, vol. 13, no. 11, pp. 2424–2436, Nov. 1996.

[18] S. Verghese, K. A. McIntosh, and E. R. Brown, "Highly tunable fiber-coupled photomixers with coherent terahertz output power," *IEEE Trans. Microw. Theory Tech.,*, vol. 45, no. 8, pp. 1301–1309, Aug. 1997.

[19] M. Tani, S. Matsuura, K. Sakai, and S. Nakashima, "Emission characteristics of photoconductive antennas based on low-temperature-grown GaAs and semi-insulating GaAs," *Appl. Opt.*, vol. 36, no. 30, pp. 7853–7859, Oct. 1997.

[20] L. Duvillaret, F. Garet, J.-F. Roux, and J.-L. Coutaz, "Analytical modeling and optimization of terahertz time-domain spectroscopy experiments using photoswitches as antennas," *IEEE J. Select. Topics Quantum Electron.*, vol. 7, no. 4, pp. 615–623, July/Aug. 2001.

[21] E. R. Brown, "THz generation by photomixing in ultrafast photoconductors," *Int. J. High Speed Electron. Syst.*, vol. 13, no. 2, pp. 497–545, 2003.

[22] G. C. Loata, M. D. Thomson, T. Loffler, and H. G. Rokos, "Radiation field screening in photoconductive antennae studied via pulsed terahertz emission spectroscopy," *App. Phys. Lett.*, vol. 91, pp. 232506, 2007.

[23] H. Roehle, R. J. B. Dietz, H. J. Hensel, J. Bttcher, H. Knzel, D. Stanze, M. Schell, and B. Sartorius, "Next generation $1.5\,\mu$m terahertz antennas: mesa-structuring of InGaAs/InAlAs photoconductive layers," *Opt. Exp.*, vol. 18, pp. 2296–2301, Feb. 2010.

[24] C. W. Berry and M. Jarrahi, "Principles of impedance matching in photoconductive antennas," *J. Infrared Milli. Terahz. Waves*, vol. 33, no. 12, pp. 1182–1189, Dec. 2012.

[25] N. Khiabani, Y. Huang, Y. Shen, and S. Boyes, "Theoretical modelling of a photoconductive antenna in a terahertz pulsed system," *IEEE Trans. Antennas Propag.*, vol. 61, no. 4, pp. 1538–1546, Apr. 2013.

[26] S. Preu, "A unified derivation of the Terahertz spectra generated by photoconductors and diodes," *J. Infrared Milli. Terahz. Waves*, vol. 35, no. 12, pp. 998–1010, Dec. 2014.

[27] S. Preu, G. H. Dhler, S. Malzer, A. Sthr, V. Rymanov, T. Gbel, E. R. Brown, M. Feiginov, R. Gonzalo, M. Beruete, and M. Navarro-Cía, "Principles of THz generation," in *Semiconductor Terahertz Technology: Devices and Systems at Room Temperature Operation*, G. Carpintero, E. García-Mũnoz, H. L. Hartnagel, S. Preu, A. V. Räisänen, Eds. Wiley, 2015, pp. 3–68.

[28] R. Emadi, N. Barani, R. Safian, A. Zeidaabadi Nezhad, "Hybrid computational simulation and study of Terahertz pulsed photoconductive antennas," *J. Infrared Milli. Terahz. Waves*, vol. 37, no. 11, pp. 1069–1085, Nov. 2016.

[29] S. J. Orfanidis, "Electromagnetic Waves and Antennas," 2013, [online] Available: http://www.ece.rutgers.edu/ orfanidi/ewa/.

[30] A. Neto and S. Maci, "Input impedance of slots printed between two dielectric media and fed by a small Δ-gap", *IEEE Antennas Wireless Propag. Lett.*, vol. 3, no. 1, pp. 113–116, Dec. 2004.

[31] A. Garufo, G. Carluccio, J. R. Freeman, D. R. Bacon, N. Llombart, E. H. Linfield, A. G. Davies, and A. Neto, "Norton equivalent circuit model for pulsed photoconductive antennas – Part II: experimental validation," *IEEE Trans. Antennas Propag.*, submitted.

[32] J. T. Darrow, X. C. Zhang, D. H. Auston, and J. D. Morse, "Saturation properties of large-aperture photoconducting antennas," *IEEE J. Quantum Electron.*, vol. 28, no. 6, pp. 1607–1616, June 1992.

[33] S. Gupta, J. F. Whitaker, and G. A. Mourou, "Ultrafast carrier dynamics in III-V semiconductors grown by molecular-beam epitaxy at very low substrate temperatures," *IEEE J. Quantum Electron.*, vol. 28, no. 10, pp. 2464–2472, Oct. 1992.

[34] D. C. Look, D. C. Walters, G. D. Robinson, J. R. Sizelove, M. G. Mier, and C. E. Stutz, "Annealing dynamics of molecular-beam epitaxial GaAs grown at 200°C," *J. Appl. Phys.*, vol. 74, no. 1, pp. 306–310, July 1993.

[35] I. S. Gregory, C. Baker, W. R. Tribe, M. J. Evans, H. E. Beere, E. H. Linfield, A. G. Davies, and M. Misssous, "High resistivity annealed low-temperature GaAs with 100 fs lifetimes," *Appl. Phys. Lett.*, vol. 83, no. 20, pp. 4199–4201, Nov. 2003.

[36] V. Ortiz, J. Nagle, J. F. Lampin, E. Peronne, and A. Alexandrou "Low-temperature-grown GaAs: Modeling of transient reflectivity experiments," *J. Appl. Phys.*, vol. 102, no. 4, pp. 043515, Aug. 2007.

[37] M. C. Nuss, D. H. Auston, and F. Capasso, "Direct subpicosecond measurement of carrier mobility of photoexcited electrons in Gallium Arsenide," *Phys. Rew. Lett.*, vol. 58, no. 22, June 1987.

[38] B. Hu, X.-C. Zhang, and D. Auston, "Temperature dependence of femtosecond electromagnetic radiation from semiconductor surfaces," *Appl. Phys. Lett.* vol. 57, no. 25, pp. 2629–2631, Dec. 1990.

[39] M. C. Beard, G. M. Turner, and C. A. Schmuttenmaer, "Subpicosecond carrier dynamics in low-temperature grown GaAs as measured by time-resolved terahertz spectroscopy," *J. Appl. Phys.*, vol. 90, no. 12, pp. 5915–5923, Dec. 2001.

[40] S. S. Prabhu, S. E. Ralph, M. R. Melloch, and E. S. Harmon, "Carrier dynamics of low-temperature-grown GaAs observed via THz spectroscopy," *Appl. Phys. Lett.*, vol. 70, no. 18, pp. 2419–2421, May 1997.

[41] J. Shan and T. F. Heinz, "Terahertz radiation from semiconductors," *Kong-Thon Tsen (Ed.): Ultrafast Dynamical Processes in Semiconductors, Topics Appl. Phys., (Springer-Verlag Berlin Heidelberg)*, vol. 92, pp. 1–59, 2004.

[42] G. C. Loata, "Investigation of low-temperature-grown GaAs photoconductive antennae for continuous-wave and pulsed terahertz generation," Ph.D. thesis, Goethe-University, Frankfut am Main, 2007.

[43] A. Papoulis, *Signal Analysis*, McGraw-Hill, New York, 1977.

[44] A. Garufo, N. Llombart, and A. Neto, "Radiation of logarithmic spiral antennas in the presence of dense dielectric lenses," *IEEE Trans. Antennas Propag.*, vol. 64, no. 10, pp. 4168–4177, Oct. 2016.

[45] [Online] CST Microwave Studio. Available at http://www.cst.com/.

[46] N. Llombart, and A. Neto, "THz time-domain sensing: The antenna dispersion and a possible solution," *IEEE Trans. THz Sci. Technol.*, vol. 2, no. 4, pp. 416–423, July 2012.

[47] S. M. Sze, "Physics of semiconductor devices," 2nd Edition, Wiley & Sons, Inc., 1981.

[48] G. Ghione, "Semiconductor device for high-speed optoelectronics," 1st Edition, Cambridge University Press, New York, 2009.

[49] A. Garufo, "Towards the engineering of pulsed photoconductive antennas," Ph.D dissertation, Dept. Microelectron., Delft Univ. of Technol., Delft, The Netherlands, 2017.

[50] B. E. A. Saleh and M. C. Teich, "Fundamentals of photonics," 2nd Edition, Wiley & Sons, Inc., 2007.

Alessandro Garufo (S'13–M'17) received the B.Sc. and M.Sc. degree in telecommunication engineering from University of Siena, Siena, Italy, in 2007 and 2012, respectively, and the Ph.D. degree in electromagnetism from Delft University of Technology, Delft, The Netherlands, in 2017.

From 2011 until 2012, he was as intern in the Antenna Group at Thales Alenia Space, Rome, Italy, where he developed his M.Sc. degree thesis. In 2012, he was a researcher in the Applied Electromagnetic Laboratory (LEA) at the University of Siena, Siena, Italy. From 2013 until 2014, he was a visiting scholar in the Metamaterials and Plasmonics Research Laboratory at University of Texas at Austin, Austin, Texas, United States of America. From 2017, he is currently a Post-Doctoral Researcher at the THz Sensing Group in the Microelectronics department of Delft University of Technology, Delft, The Netherlands. His research interest includes analysis and design of antennas, dielectric lens antennas and antenna arrays with emphasis at THz frequencies based on photoconductive sources.

Giorgio Carluccio was born in 1979 and grew up in Ortelle, Lecce, Italy. He received the Laurea degree in telecommunications engineering and the Ph.D. degree in information engineering from the University of Siena, Siena, Italy, in 2006 and 2010, respectively.

From October 2008 to March 2009 he was an Invited Visiting Scholar with the ElectroScience Laboratory, Department of Electrical and Computer Engineering, at The Ohio State University, Columbus, Ohio, USA. From February 2010 to January 2012 and from July 2013 to July 2014, he was a Postdoctoral Research Associate with the Department of Information Engineering and Mathematics at the University of Siena. From April 2012 to March 2013, he was a Postdoctoral Research Associate with the Department of Electronics and Telecommunication at the University of Firenze, Firenze, Italy. During 2012 and 2013 he also spent some months as a visiting Post-Doc Researcher with the Department of Microelectronics at the Delft University of Technology (TU Delft), Delft, The Netherlands. Since September 2014 he has been a Post-Doc Researcher with the Department of Microelectronics at TU Delft. His research interests deal with electromagnetic wave theory, mainly focused on asymptotic high-frequency techniques for electromagnetic scattering and propagation. He also worked on the modeling and design of dielectric lens antennas, reflectarray antennas, and THz antennas based on photoconductive materials.

Nuria Llombart (S'06–M'07–SM'13) received the Electrical Engineering and Ph.D. degrees from the Polytechnic University of Valencia, Spain, in 2002 and 2006, respectively.

During her Master's degree studies she spent one year at the Friedrich-Alexander University of Erlangen-Nuremberg, Germany, and worked at the Fraunhofer Institute for Integrated Circuits, Erlangen, Germany. From 2002 until 2007, she was with the Antenna Group, TNO Defence, Security and Safety Institute, The Hague, The Netherlands, working as a Ph.D. student and afterwards as a Researcher. From 2007 until 2010, she was a Postdoctoral Fellow at the California Institute of Technology, working for the Sub millimeter Wave Advance Technology Group, Jet Propulsion Laboratory, Pasadena, USA. She was a Ramn y Cajal Fellow at the Optics Department of the Complutense University of Madrid, Spain, from 2010 to 2012. In September 2012, she joined the THz Sensing Group at Delft University of Technology, Delft, The Netherlands, where she is currently an Associate Professor.

She has co-authored over 150 journal and international conference contributions. Her research interests include the analysis and design of planar antennas, periodic structures, reflector antennas, lens antennas, and waveguide structures, with emphasis in the THz range. Dr. Llombart was co-recipient of the H.A. Wheeler Award for the Best Applications Paper of the year 2008 in the IEEE TRANSACTIONS ON ANTENNAS AND PROPAGATION and the 2014 Best Paper Award in the IEEE TRANSACTION ON THZ SCIENCE AND TECHNOLOGY and several NASA awards. She also received the 2014 IEEE Antenna and Propagation Society Lot Shafai Mid-Career Distinguished Achievement Award. She served as Associate Editor of the IEEE LETTERS ON ANTENNAS AND PROPAGATION and the IEEE ANTENNAS AND PROPAGATION MAGAZINE, she also served as Topical Editor of the IEEE TRANSACTION ON TERAHERTZ SCIENCE AND TECHNOLOGY. She serves as a Board Member of the IRMMW-THz International Society. In 2015, she was awarded with an European Research Council (ERC) Starting Grant.

Andrea Neto (M'00−SM'10−F'16) received the Laurea degree (*summa cum laude*) in electronic engineering from the University of Florence, Florence, Italy, in 1994, and the Ph.D. degree in electromagnetics from the University of Siena, Siena, Italy, in 2000. Part of his Ph.D. degree was developed at the European Space Agency Research and Technology Center, Noordwijk, The Netherlands, where he was involved in the antenna section for over two years.

From 2000 to 2001, he was a Post-Doctoral Researcher with the California Institute of Technology, Pasadena, CA, USA, where he was involved in the Sub-Millimeter-Wave Advanced Technology Group. From 2002 to 2010, he was a Senior Antenna Scientist at TNO Defence, Security, and Safety, The Hague, The Netherlands. In 2010, he was appointed Full Professor of Applied Electromagnetism in the Electrical Engineering, Mathematics and Computer Science Faculty of Delft University of Technology, Delft, The Netherlands, where he formed and leads the THz Sensing Group. His current research interests are in the analysis and design of antennas, with emphasis on arrays, dielectric lens antennas, wideband antennas, electromagnetic band-gap structures, and terahertz antennas.

Dr. Neto was a co-recipient of the H. A. Wheeler Award for the best applications paper of the year 2008 in the IEEE TRANSACTIONS ON ANTENNAS AND PROPAGATION, the Best Innovative Paper Prize at the 30th ESA Antenna Workshop in 2008, the Best Antenna Theory Paper Prize at the European Conference on Antennas and Propagation in 2010. In 2011, he was awarded the European Research Council Starting Grant to perform research on Advanced Antenna Architectures for THz Sensing Systems. He is member of the Technical Board of the European School of Antennas and organizer of the course on Antenna Imaging Techniques. He is a member of the steering committee of the network of excellence NEWFOCUS, dedicated to focusing techniques in mm and sub-millimeter-wave regimes. He was the Awards and Grants Chair of the European Conference on Antennas and Propagation in 2014. He served as an Associate Editor of the IEEE TRANSACTIONS ON ANTENNAS AND PROPAGATION from 2008 to 2013, and the IEEE ANTENNAS AND WIRELESS PROPAGATION LETTERS from 2005 to 2013. He serves as an Associate Editor of the IEEE TRANSACTIONS ON TERAHERTZ SCIENCE AND TECHNOLOGY.